JOURNAL OF SOLID STATE CHEMISTRY 86, 1–15 (1990)

Structural Properties of Transition Metal Pyroarsenates $M_2As_2O_7$ (M = Co, Mn, Ni)

A. M. BUCKLEY,[1] S. T. BRAMWELL,[2] AND P. DAY[2]

Inorganic Chemistry Laboratory, South Parks Road, Oxford OX1 3QR, United Kingdom

Received October 26, 1989

Single phase powder samples of the transition metal pyroarsenates, $M_2As_2O_7$ (M = Co, Mn, Ni), have been prepared and analyzed by X-ray diffraction, chemical analysis, high resolution powder neutron diffraction, and differential scanning calorimetry measurements. $Co_2As_2O_7$ and $Ni_2As_2O_7$ were found to undergo high temperature structural phase transitions between α- and β-forms at 452 and 691 K, respectively. The high temperature β-modifications of $Co_2As_2O_7$ and $Ni_2As_2O_7$ are isomorphous with $Sc_2Si_2O_7$ (thortveitite) of space group $C2/m$, with cell constants a = 6.6316(1) Å, b = 8.5541(1) Å, c = 4.7633(1) Å, β = 103.56(1)°, and a = 6.5391(1) Å, b = 8.5007(1) Å, c = 4.7437(1) Å, β = 103.19(1)°, respectively. $Mn_2As_2O_7$ does not exhibit a high temperature phase transition and adopts the thortveitite structure at room temperature; a = 6.7442(2) Å, b = 8.7545(3) Å, c = 4.8025(2) Å, β = 102.76(1)°. The structures of all three thortveitite phases have been refined, and positional and thermal parameters are given. The α-$M_2As_2O_7$ (M = Co, Ni) are triclinic ($P1$ or $P\bar{1}$) but the structures could not be refined satisfactorily from powder neutron data.

1. Introduction

Crystals of composition $X_2Y_2O_7$ (X = K, Rb, Ca, Sr, Cd, Mg, Ni, Co, Zn, Mn, Cu, Sc; Y = Cr, V, As, P, Si, S) belong to a small number of groups of related structures (*1*). Compounds where the ionic radius of the Y atom, $r(Y)$, is less than 0.60 Å, crystallize into structures analogous to those of pyrochlore and weberite in which Y is octahedrally coordinated (*2*). In the remainder, Y occurs in tetrahedral coordination and the compounds tend to adopt either the thortveitite ($Sc_2Si_2O_7$) structure (*3*) ($r(X) < 0.97$ Å) or one of the so-called "dichromate" structures ($r(X) > 0.97$ Å) (*1*). In these cases the crystals may be formulated as ionic with X^{n+} as the cation and $Y_2O_7^{n-}$, in which two YO_4 tetrahedra share an oxygen atom, as the anion. In the dichromate structures the anion occurs in an eclipsed configuration with a Y–O–Y angle of ~130°, while in the thortveitite structure it is staggered with a Y–O–Y angle of 180°.

A number of pyroarsenates and pyrophosphates $M_2^{II}Y_2O_7$ (M = Ni, Mg, Co, Zn, Cu; Y = As, P) occur in two polymorphs; a low temperature α-phase and a high temperature β-phase. The β-phase always adopts the thortveitite structure with a linear Y–O–Y group whereas the α-phase is always a close modification of the thort-

[1] To whom correspondence should be addressed at present address: Research and Technology, ICI Chemicals and Polymers Ltd., P.O. Box 8, The Heath, Runcorn, Cheshire WA7 4QD, United Kingdom

[2] Present address: Institut Laue-Langevin, 156X, 38042 Grenoble Cedex, France.

0022-4596/90 $3.00

veitite structure with a bent Y–O–Y linkage. There has been much interest in the nature of the α–β structural phase transition in these compounds and its relation to the bridging oxygen of the Y–O–Y group (*4*).

In the present paper we describe the preliminary results of an investigation of the structural properties of $M_2As_2O_7$ (M = Co, Mn, Ni). We note that the magnetic properties of these compounds (*5*), α-$Co_2P_2O_7$ (*6*) and $Mn_2P_2O_7$ (*7*), have also been studied. The compounds are all antiferromagnetic, adopting a variety of low-temperature magnetic structures.

Previous attempts to produce pure powder samples of $M_2As_2O_7$ (M = Ni, Co) have resulted in mixtures of metal arsenates (*8*). We have found a very simple way of avoiding this problem and the present paper reports the preparation and structural characterization of single phase samples of $M_2As_2O_7$ (M = Co, Mn, Ni).

2. Experimental

2.1 Preparations

2.1(i) Nickel pyroarsenate. Nickel pyroarsenate was prepared by adapting the preparation of Taylor and Heyding (*8*). As_2O_5 (6.75 g; 0.03 moles) and $Ni(NO_3)_2$ (11.64 g; 0.04 moles) were carefully ground together and placed in a porcelain crucible. Small quantities of As_2O_5 were sprinkled onto the top of the mixture in an effort to maintain a significant vapor pressure of As in the crucible, and so prevent the evaporation of As from the reaction mixture. The crucible was placed in a muffle oven at 900°C for 2 hr and then cooled to room temperature over 3 hr.

Addition of excess As_2O_5 prevented the formation of arsenic-deficient impurities such as $Ni_3(AsO_4)_2$, as was formed from Taylor and Heyding's preparation (*8*). The powder was removed from the crucible and washed with hot distilled water to remove excess unreacted As_2O_5, the suspension filtered and the solid dried in air. The product was a golden yellow microcrystalline powder.

2.1(ii) Cobalt pyroarsenate. Cobalt pyroarsenate was prepared by a similar method to that of the nickel analog. As_2O_5 (14.69 g; 0.064 moles) and $Co(NO_3)_2$ (17.64 g; 0.06 moles) were ground together and placed in a platinum crucible. Again, excess As_2O_5 was sprinkled on the surface of the reactants in the crucible to prevent the formation of a pink, arsenic-deficient impurity, $Co_3(AsO_4)_2$. The crucible was placed in a muffle oven at 900°C for 2 hr and then cooled at room temperature over 3 hr. After removal from the crucible, the product was washed with hot distilled water to remove excess As_2O_5. A dark purple microcrystalline powder resulted.

2.1(iii) Manganese pyroarsenate. Manganese pyroarsenate was prepared by heating a porcelain crucible containing synthetic krautite, $HMnAsO_4 \cdot H_2O$, in a muffle oven at 600°C for 4 hr (*9*). The sample of krautite had been prepared following the method of Buckley (*5*).

2.2 Characterization

Small quantities of the products prepared in Section 2.1 were analyzed by atomic absorption spectroscopy using a Perkin–Elmer 8000 spectrometer.

X-ray diffraction profiles of the samples were obtained using a Philips PW1729 diffractometer controlled by a Philips 1710 microprocessor and minicomputer. All patterns were recorded at room temperature using Cu$K\alpha$ radiation of wavelength 1.541 Å. Powder data were analyzed using the X-ray powder pattern least-squares refinement program REFCEL (*10*) on the Oxford University VAX Cluster computer. This program refines the cell constants and zero point for a given set of reflections and their 2θ angles.

TABLE I

CHEMICAL ANALYSIS OF TRANSITION METAL PYROARSENATES $M_2As_2O_7$

Metal	% M by weight	% As by weight
Co	30.78(31.03)	39.12(39.43)
Ni	30.81(30.96)	40.38(39.43)
Mn	28.28(29.55)	41.08(40.31)

Differential scanning calorimetry (DSC) measurements were made on the samples using a Perkin–Elmer 7 Series thermal analysis system (Co and Ni compounds) and a DuPont 9000 thermal analyzer with a 910 DSC module (Mn compound), by members of the Characterisation and Measurement Group, ICI Chemicals and Polymers Ltd., Runcorn, U.K.

2.3 Powder Neutron Diffraction

Data were collected on the High Resolution Powder Diffractometer (HRPD) (*11*) at the Rutherford Appleton Laboratory (RAL), Didcot, Oxon, U.K. About 7 g of each of the samples was contained in rectangular vanadium cans inside a RAL furnace with vanadium windows. Data were collected for $Mn_2As_2O_7$ between times of flight of 30–130 msec (d-spacing range of 0.6–2.6 Å) at room temperature. High temperature profiles were obtained for $Co_2As_2O_7$ at 250°C and $Ni_2As_2O_7$ at 500°C between times of flight of 30–130 msec. Room temperature profiles were also collected for $Ni_2As_2O_7$ (between times of flight of 30–130 msec) and $Co_2As_2O_7$ between times of flight of 30–280 msec (d-spacing range of 0.6–5.6 Å). After heating in the furnace the nickel and cobalt compounds were examined by X-ray diffraction to ensure that they had not cooled into new structural phases or been contaminated at high temperatures. The X-ray profiles of both compounds were exactly the same as those obtained before the experiment. The diffraction profiles were normalized by fitting a polynomial to the incident background shape and refined using the Rietveld profile refinement technique (*12*) modified for a pulsed neutron source (*13*).

3. Results

3.1 Characterization

The analytical results for $M_2As_2O_7$ are given in Table I. The numbers in parentheses are the theoretical percentage weights.

The room temperature X-ray diffraction profiles of the three compounds are shown in Fig. 1. The lattice constants, determined using REFCEL (*10*), are given in Table II, and the indexing of the X-ray diffraction profiles of the samples is given in the Appendix. The diffraction profiles of $Co_2As_2O_7$ and $Ni_2As_2O_7$, whose room temperature structures are considered to be isomorphous (*8*, *14*), were indexed using a triclinic cell in accordance with the lattice given by Ozog *et al.* (*14*) for $Co_2As_2O_7$. The tetragonal cell for $Co_2As_2O_7$ and $Ni_2As_2O_7$ proposed by Taylor and Heyding (*8*) was not used. The X-ray profiles they obtained were poorly defined since their sample appeared to be contaminated with other arsenates.

No powder diffraction data have been published to date for $Mn_2As_2O_7$ so the X-

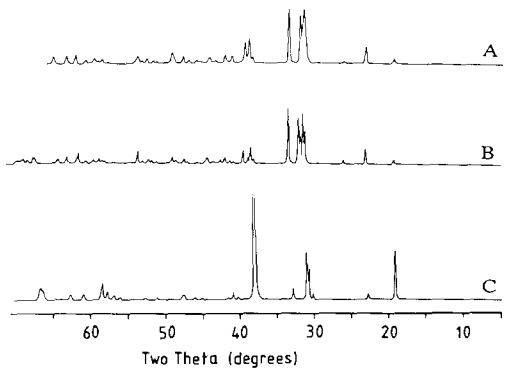

FIG. 1. Powder X-ray diffraction profiles of (a) $Ni_2As_2O_7$, (b) $Co_2As_2O_7$, and (c) $Mn_2As_2O_7$.

TABLE II

LATTICE CONSTANTS FOR $M_2As_2O_7$ AT 300 K DETERMINED BY POWDER X-RAY DIFFRACTION

M	Space group	a_0	b_0 (Å)	c_0	α	β (°)	γ	No. of reflections fitted
Co	$P1$	6.555(5)	8.521(5)	4.759(3)	91.00(4)	104.00(5)	91.29(3)	34
Mn	$C2/m$	6.745(8)	8.757(9)	4.803(7)	90.00	102.8(1)	90.00	22
Ni	$P1$	6.558(8)	8.55(1)	4.712(5)	91.01(5)	103.98(7)	91.29(8)	37

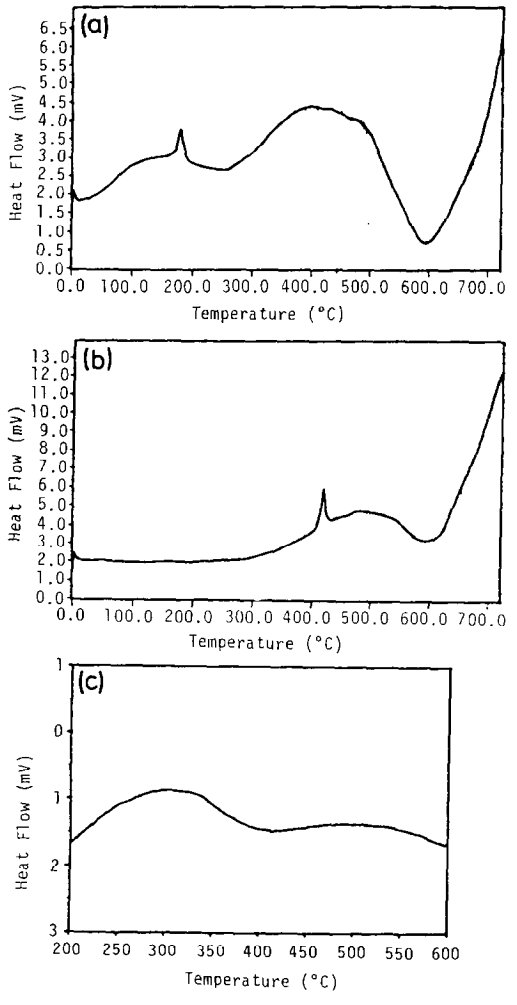

FIG. 2. DSC runs for (a) $Co_2As_2O_7$, (b) $Ni_2As_2O_7$, and (c) $Mn_2As_2O^7$.

ray diffraction profile was indexed using a C-centered monoclinic cell by analogy with $Mn_2P_2O_7$ and $Mg_2As_2O_7$ whose unit cells are monoclinic (*15, 16*).

The DSC scans for all three pyroarsenates are shown in Fig. 2 and Table III gives the conditions for the measurements and details of any peaks observed. The DSC scans for $Co_2As_2O_7$ and $Ni_2As_2O_7$ reveal positive signals at around 452 and 692 K, respectively, corresponding to endothermic heat changes. The former has 2.85 kJ/mol and the latter 4.44 kJ/mol associated with it. No such peak is observed for $Mn_2As_2O_7$.

3.2 Crystal Structure Refinement

Comparison between the high resolution powder neutron diffraction profiles obtained for the compounds $M_2As_2O_7$ (M = Co, Mn, Ni) shows that for $Co_2As_2O_7$ and $Ni_2As_2O_7$, a structural phase transition occurs on cooling from high to room temperature. This is probably associated with a lowering of the symmetry of the unit cell. The neutron diffraction profile of $Mn_2As_2O_7$ at room temperature is very similar to those

TABLE III

DIFFERENTIAL SCANNING CALORIMETRY RESULTS FOR $M_2As_2O_7$ (M = Co, Mn, Ni)

M	T_1 (K)	T_2 (K)	T_{max} (K)	Area (mJ)	ΔH (J/g)	ΔH (J/g)
Co	428.6	482.3	452.4	72.22	7.51	2.85
Ni	670.0	707.2	691.9	113.89	11.72	4.44

of $Co_2As_2O_7$ and $Ni_2As_2O_7$ at 250 and 500°C, respectively. This high resolution powder neutron diffraction data was used to refine the crystal structures of the $M_2As_2O_7$ compounds.

3.2(i) High Temperature Phases of $Co_2As_2O_7$ and $Ni_2As_2O_7$

The thortveitite structure was used as a starting model for the profile refinement of the high temperature structures of $Co_2As_2O_7$ and $Ni_2As_2O_7$ at 250 and 500°C, respectively (henceforth referred to as β-$Co_2As_2O_7$ and β-$Ni_2As_2O_7$).

The lattice dimensions and atom positions of $Mg_2As_2O_7$ (*16*) were used. The background was refined by fitting a fifth order Chebyschev polynomial. In both cases the program VDLSQ, which is contained in the Cambridge Crystallography Subroutine Library (CCSL) (*17*), was used. This program has as its peak shape function the convolution of a Gaussian with a Lorentzian (Voigt function) and two decaying exponential functions (*18*). The Voigt profile shape function was used to describe the significant peak broadening observed.

The refinements converged with $\chi^2 = 3.4$, $R_n = 9.2\%$, $R_p = 4.6\%$, and $R_{wp} = 5.8\%$ for β-$Ni_2As_2O_7$ and $\chi^2 = 2.0$, $R_n = 10.0\%$, $R_p = 3.6\%$, and $R_{wp} = 4.5\%$ for β-$Co_2As_2O_7$ (terms described in Ref. (*18*)), using isotropic thermal factors. When the anisotropic thermal factors were allowed to vary, the fits improved in both cases to $\chi^2 = 2.2$, $R_n = 6.9\%$, $R_p = 3.7\%$, and $R_{wp} = 4.6\%$ for β-$Ni_2As_2O_7$ and $\chi^2 = 1.5$, $R_n = 6.1\%$, $R_p = 3.2\%$, and $R_{wp} = 3.9\%$ for β-$Co_2As_2O_7$. Significance tests (*19*) indicated that the improvements in both cases were significant to 99.5% confidence limits. Large values of the anisotropic temperature factors B_{22} and B_{33} for the bridging oxygen, O1, of the As_2O_7 group, were observed. The fits obtained are shown in Figs. 3 and 4. Tables IV and V contain structural data for the two compounds.

3.2(ii) Room Temperature Structure of $Mn_2As_2O_7$

By analogy with $Mn_2P_2O_7$ and $Mg_2As_2O_7$, which also do not exhibit high temperature structural phase transitions, the space group of $Mn_2As_2O_7$ was expected to be $C2/m$. All the observed peaks were indexed in this space group. Accurate unit cell constants of the monoclinic cell of $Mn_2As_2O_7$ were obtained using the least-squares fitting program D5LSQ (CCSL) which refines unit cell constants for a given set of reflections and their times of flight.

The crystal structure of $Mn_2As_2O_7$ was then refined by the Rietveld method for a pulsed neutron source using the program VDLSQ. The background was refined by fitting to a fifth order Chebyschev polynomial. Anisotropic temperature factors were again used for all the atoms in the unit cell. The refinement converged at $\chi^2 = 12.6$, $R_n = 13\%$, $R_p = 7.8\%$, and $R_{wp} = 9\%$. Anisotropic temperature factors B_{22} and B_{33} for the bridging oxygen O1 of the As_2O_7 group were found to be large. The fit obtained is given in Fig. 5 and structural data in Tables VI and VII.

That the refinement converged to rather higher R-factors than is usual is probably due to anisotropic peak broadening that is not satisfactorily modeled by the Voigt function. Lowering the symmetry of the unit cell did not improve the fit. Furthermore, comparison of the F_{obsd} and F_{calcd} Fourier sections revealed that no scattering density was unaccounted for. Hence, the refinement is considered to be a solution of the structure although the fit is limited by sample effects.

3.2(iii) Room Temperature Structures of $Co_2As_2O_7$ and $Ni_2As_2O_7$

The room temperature powder neutron diffraction profile indicates that the unit cell of α-$Co_2As_2O_7$ has lower symmetry than that of β-$Co_2As_2O_7$. Furthermore, Ozog *et*

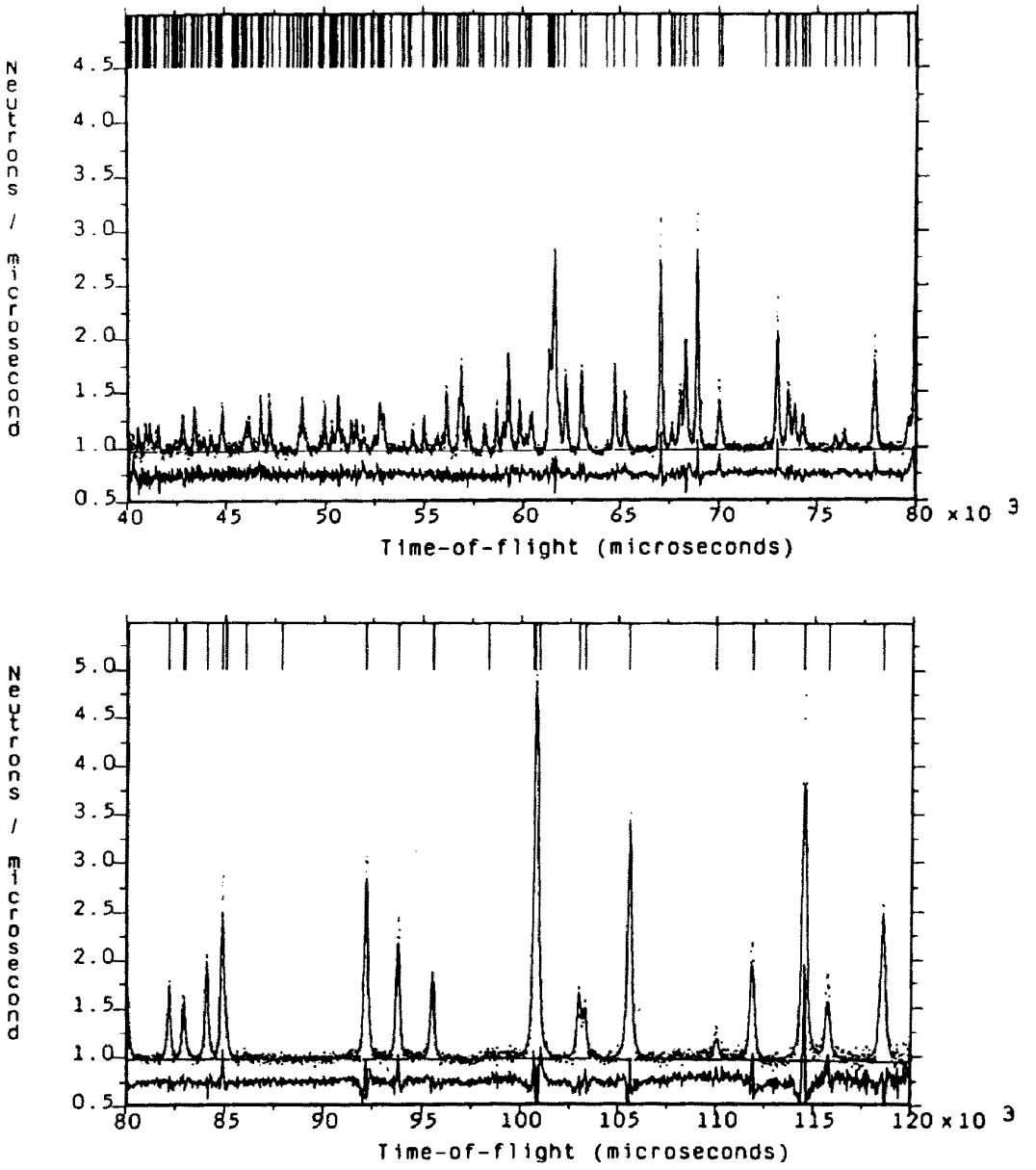

FIG. 3. Observed (dots) and calculated (full line) neutron diffraction profiles of β-$Co_2As_2O_7$. Lower line is difference and tags mark positions of reflections.

al. (*14*) obtained Weissenberg photographs from a single crystal of $Co_2As_2O_7$ at room temperature and concluded that the unit cell was triclinic ($C1$ or $C\bar{1}$). Hence, the starting model was deduced from the β-$Co_2As_2O_7$ unit cell ($C2/m$) by removing all the elements of symmetry and thereby creating 22 atom positions and the lattice constants obtained by Ozog *et al.* (*14*). The best fit had $\chi^2 = 11$, $R_n = 27\%$, $R_p = 11\%$,

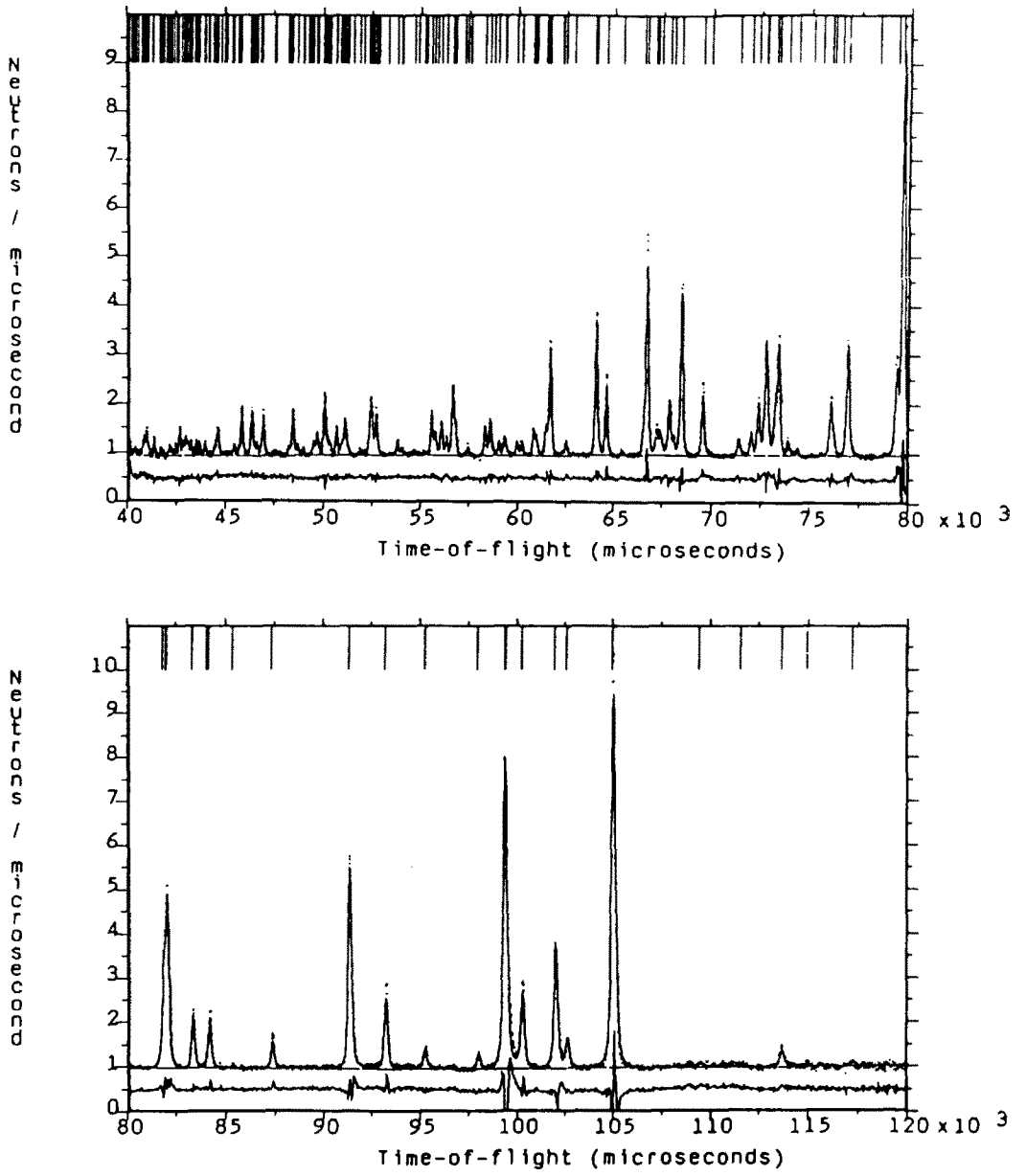

FIG. 4. Observed (dots) and calculated (full line) neutron diffraction profiles of β-$Ni_2As_2O_7$. Lower line is difference and tags mark positions of reflections.

and R_{wp} = 12%. The intensities of the majority of peaks were incorrect. Furthermore, there were some observed peaks not predicted by the structural model given above. The latter were not considered to be due to an impurity because the 250°C neutron profile and the X-ray pattern after the experiment showed no evidence of any.

Further attempts were made to deduce the space group and unit cell constants of

TABLE IV

CRYSTALLOGRAPHIC DATA FOR β-$Co_2As_2O_7$ AND β-$Ni_2As_2O_7$

	β-$Co_2As_2O_7$	β-$Ni_2As_2O_7$
Space group	$C2/m$	$C2/m$
Axes	a = 6.6316(1) Å	a = 6.5391(1) Å
	b = 8.5541(1) Å	b = 8.5007(1) Å
	c = 4.7633(1) Å	c = 4.7437(1) Å
	β = 103.56(1)°	β = 103.19(1)°

Positional parameters

(a) β-$Co_2As_2O_7$

	x/a	y/b	z/c	B_{iso} (Å^2)
Co	0	0.3123(4)	0.5	0.2(1)
As	0.2246(2)	0	0.9047(3)	−1.07(3)
O1	0	0	0	0.09(3)
O2	0.3960(2)	0	0.2252(3)	−0.37(4)
O3	0.2310(2)	0.1620(1)	0.7130(2)	0.09(3)

(b) β-$Ni_2As_2O_7$

Ni	0	0.3136(1)	0.5	0.17(3)
As	0.2263(2)	0	0.9030	−0.73(3)
O1	0	0	0	6.9(1)
O2	0.3983(2)	0	0.2303(3)	0.32(4)
O3	0.2315(2)	0.1648(1)	0.7129(2)	0.80(4)

Anisotropic thermal factors for β-$Co_2As_2O_7$

Atom	B_{11}	B_{22}	B_{33}	B_{23}	B_{13}	B_{12}
Co	1.8(2)	0.5(2)	3.2(2)	0	0.2(1)	0
As	0.6(1)	0.6(1)	0.4(1)	0	−0.11(5)	0
O(1)	1.3(2)	16.1(4)	8.2(3)	0	2.0(1)	0
O(2)	2.40(9)	0.93(7)	0.73(7)	0	−0.24(7)	0
O(3)	3.36(7)	1.42(5)	0.85(5)	0.24(4)	0.32(4)	0.65(6)

Anisotropic thermal factors for β-$Ni_2As_2O_7$

Atom	B_{11}	B_{22}	B_{33}	B_{23}	B_{13}	B_{12}
Ni	2.14(4)	0.91(4)	1.74(4)	0	−0.20(3)	0
As	1.07(5)	0.86(6)	0.44(6)	0	−0.65(5)	0
O(1)	1.9(2)	14.0(4)	10.7(3)	0	2.1(1)	0
O(2)	2.65(8)	1.16(7)	0.67(6)	0	−0.56(6)	0
O(3)	3.20(6)	1.66(5)	1.74(6)	0.79(4)	0.25(4)	0.46(4)

Note. The temperature factor has the form $\exp[-\frac{1}{4}\{B_{11}h^2a^{*2} + \ldots 2B_{12}hka^*b^* + \ldots\}]$.

β-$Co_2As_2O_7$. The extra peaks could not be indexed in space groups $P1$ or $P2_1/c$ with the original $C2/m$ cell constants. Combinations of doubled unit cell constants in space group P1 were tried but none of these trials would account for the unpredicted observed peaks. The autoindexing program of Visser (*20*) yielded no sensible solutions for 30 reflections between times of flight of 60–

TABLE V

INTERATOMIC DISTANCES FOR β-$Co_2As_2O_7$ AND β-$Ni_2As_2O_7$

Atoms	Bond length (Å)	Atoms	Bond angle (°)
	β-$Co_2As_2O_7$		
As_2O_7 group			
As–O1[a]	1.656(2)	O1–As–O2	102.2(1)
As–O2[a]	1.676(2)	O1–As–O3	106.89(7)
As–O3	1.666(1)	O2–As–O3	113.60(6)
		O3–As–O3	112.6(1)
		As–O1–As	180.0(0)
O1–O2	2.594(1)		
O1–O3[b]	2.668(1)		
O2–O3[c]	2.790(2)		
O3–O3[d]	2.772(2)		
CoO_6 group			
Co–O2[e]	2.084(3)	O2–Co–O3	151.96(8)
Co–O3	2.074(2)	O2–Co–O3	79.80(8)
Co–O3[e]	2.260(1)	O2–Co–O2	79.2(1)
		O2–Co–O3	94.16(4)
Co–Co[d]	3.211(7)	O3–Co–O3	168.8(2)
		O3–Co–O3	114.26(8)
		Co–O2–Co	100.8(1)
		Co–O3–Co	106.88(5)
	β-$Ni_2As_2O_7$		
As_2O_7 group			
As–O1[a]	1.647(1)	O1–As–O2	101.22(9)
As–O2[a]	1.697(1)	O1–As–O3	106.33(7)
As–O3	1.671(1)	O2–As–O3	113.77(6)
		O3–As–O3	114.0(1)
		As–O1–As	180.0(0)
O1–O2	2.584(1)		
O1–O3[b]	2.655(1)		
O2–O3[c]	2.756(2)		
O3–O3[d]	2.802(2)		
NiO_6 group			
Ni–O2[e]	2.050(1)	O2–Ni–O3	151.79(5)
Ni–O3	2.053(1)	O2–Ni–O3	80.21(5)
Ni–O3[e]	2.224(1)	O2–Ni–O2	78.75(6)
		O2–Ni–O3	94.10(3)
Ni–Ni[d]	3.169(2)	O3–Ni–O3	170.53(6)
		O3–Ni–O3	113.42(5)
		Ni–O2–Ni	101.25(6)
		Ni–O3–Ni	107.20(4)

Note. Equivalent positions: (*a*) $x, y, z + 1$; (*b*) $x, y, -z$; (*c*) $-x, y, -z$; (*d*) $x, -y, z$; (*e*) $-(x + \frac{1}{2}), -y + \frac{1}{2}, z$.

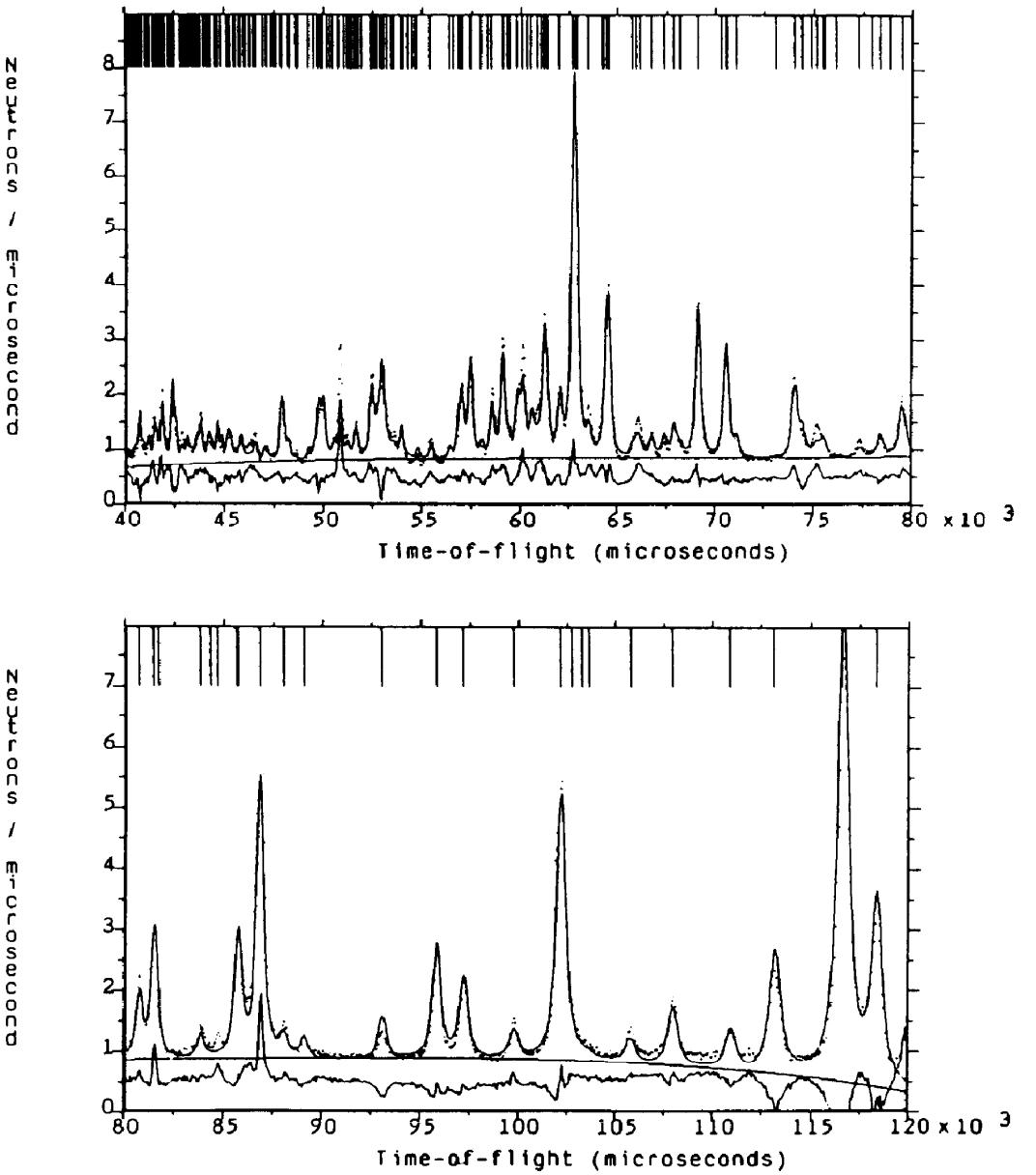

FIG. 5. Observed (dots) and calculated (full line) neutron diffraction profiles of $Mn_2As_2O_7$ using Voigt profile function and anisotropic thermal factors. Lower line is difference and tags mark the positions of the reflections.

140 msec. In an attempt to measure the low order reflections and thereby deduce the unit cell, a neutron diffraction profile was obtained at longer times of flight, 140–280 msec (i.e., greater *d*-spacing; 2.8–5.6 Å). No extra reflections were observed that could not be indexed on the original triclinic unit cell.

TABLE VI

CRYSTALLOGRAPHIC DATA FOR $Mn_2As_2O_7$

Space group		$C2/m$		
Axes		a = 6.7442(2) Å		
		b = 8.7545(3) Å		
		c = 4.8025(2) Å		
		β = 102.76(1)°		
Atom	x/a	y/b	z/c	B_{iso} (Å^2)
Mn	0	0.3110(4)	0.5	1.1(2)
As	0.2268(3)	0	0.9062(7)	−0.2(1)
O1	0	0	0	6.4(4)
O2	0.3977(5)	0	0.2156(8)	−0.7(1)
O3	0.2336(3)	0.1582(3)	0.7107(6)	0.18(9)

Anisotropic temperature factors

Atom	B_{11}	B_{22}	B_{33}	B_{23}	B_{13}	B_{12}
Mn	0.00	−1.7(2)	9.7(5)		−1.9(3)	
As	−2.1(1)	1.0(1)	2.2(2)		−0.5(1)	
O1	0.8(3)	14.7(8)	8.1(6)		5.4(3)	
O2	0.1(1)	−0.1(1)	2.8(2)		−2.5(2)	
O3	−0.6(1)	0.3(1)	4.2(2)	0.00	−2.0(1)	0.8(1)

Note. The temperature factor has the form $\exp[-\frac{1}{4}\{B_{11}h^2a^{*2} + \ldots 2B_{12}hka^*b^* + \ldots\}]$.

TABLE VII

INTERATOMIC DISTANCES AND ANGLES FOR $Mn_2As_2O_7$

Atoms	Bond length (Å)	Atoms	Bond angle (°)
As_2O_7 group			
As–O1[a]	1.687(3)	O1–As–O2	104.5(9)
As–O2[a]	1.67(3)	O1–As–O3	106.7(1)
As–O3	1.679(3)	O2–As–O3	113.5(4)
		O3–As–O3	111.1(3)
		As–O1–As	180.0(0)
O1–O2	2.635(3)		
O1–O3[b]	2.715(3)		
O2–O3[c]	2.794(4)		
O3–O3[d]	2.783(4)		
MnO_6 group			
Mn–O2[e]	2.16(2)	O2–Mn–O3	151.2(4)
Mn–O3	2.143(3)	O2–Mn–O3	78.5(6)
Mn–O3[e]	2.265(3)	O2–Mn–O2	80(1)
		O2–Mn–O3	94.6(4)
Mn–Mn[d]	3.309(7)	O3–Mn–O3	166.3(2)
		O3–Mn–O3	115.9(1)
		Mn–O2–Mn	100(1)
		Mn–O3–Mn	106.7(1)

Note. Equivalent positions: (*a*) $x, y, z + 1$; (*b*) $x, y, -z$; (*c*) $-x, y, -z$; (*d*) $x, -y, z$; (*e*) $-(x + \frac{1}{2}), -y + \frac{1}{2}, z$.

The structure of α-$Ni_2As_2O_7$ was considered to be isomorphous with that of α-$Co_2As_2O_7$ (*8*). Furthermore, the X-ray diffraction profiles of the two compounds are very similar (Fig. 1). As was the case for α-$Co_2As_2O_7$, the structure of α-$Ni_2As_2O_7$ was considered to be closely related to that of thortveitite but of lower symmetry. The same starting model as used for α-$Co_2As_2O_7$ was employed in the refinement. The refinement converged with very large R-factors, R_n = 26%, R_p = 13%, and R_{wp} = 16%, for reasons similar to those that prevented full refinement of the α-$Co_2As_2O_7$ data. The predicted intensities of the model were too low for most reflections and some observed peaks were not predicted by the model.

The similarity between the fits indicates that both structures are closely related to their high temperature analogs and hence to the parent compound thortveitite. The presence of unpredicted peaks in both refinements indicates that the unit cell and space group are incorrect, although the symmetry is unlikely to be anything other than triclinic, as the structure is clearly almost correct. It would appear that some subtle combination of any number of the unit cell axes has occurred. In the future we intend to obtain high resolution X-ray diffraction profiles of α-$Co_2As_2O_7$ and α-$Ni_2As_2O_7$ in order to measure the lowest order reflections which are not obtainable using HRPD. It may then be possible to establish the unit cells of the compounds by auto-indexing methods.

4. Discussion

For the first time we have prepared single phase samples of the transition metal pyroarsenates, $M_2As_2O_7$ (M = Co, Mn, Ni). A previous attempt to prepare them resulted in mixtures that were at least biphasic (*8*) and this lead to an incorrect assignment of the unit cell from powder X-ray diffraction data. In the present work powder X-ray dif-

fraction profiles have been successfully indexed on the basis of monoclinic ($Mn_2As_2O_7$) and triclinic (α-$Co_2As_2O_7$, α-$Ni_2As_2O_7$) unit cells, although the full crystal structures of the latter two compounds remain to be established. Powder neutron diffraction experiments have shown that $Co_2As_2O_7$ and $Ni_2As_2O_7$ undergo high temperature structural phase transitions in common with other $M_2X_2O_7$ compounds. Endothermic signals in the DSC traces of $Co_2As_2O_7$ and $Ni_2As_2O_7$ are observed at 452 and 691 K, respectively, and almost certainly correspond to the α–β-phase transition.

4.1 The Crystal Structures of β-$Co_2As_2O_7$, β-$Ni_2As_2O_7$, and $Mn_2As_2O_7$

We have shown that β-$Co_2As_2O_7$, β-$Ni_2As_2O_7$, and $Mn_2As_2O_7$ are isomorphous and adopt the thortveitite structure, of which $Sc_2Si_2O_7$ is the parent compound. The essential features of the structure are as follows: the M^{2+} (M = Co, Mn, Ni) octahedra share edges in a hexagonal arrangement in the *ab*-plane, as depicted in Fig. 6, forming a distorted honeycomb arrangement of M^{2+} ions. The arsenate sheets are packed in such a way that an As ion on one side of the As_2O_7 group shares one oxygen atom from the NiO_6 sheet above and two oxygen atoms from the NiO_6 below, in the

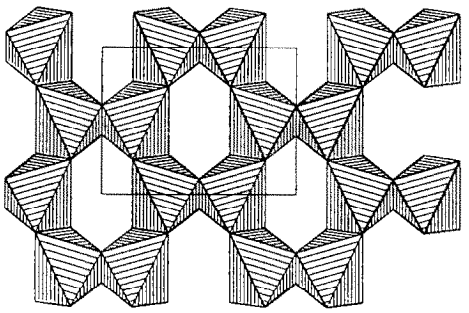

FIG. 6. Projection on the (0 0 1) plane of β-$Ni_2As_2O_7$, β-$Co_2As_2O_7$, and $Mn_2As_2O_7$ showing the hexagonal arrangement of MO_6 octahedra.

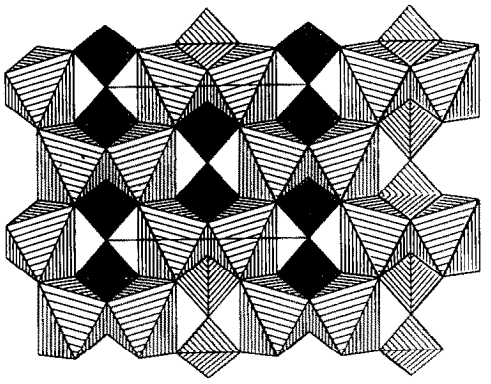

FIG. 7. Projection on the (0 0 1) plane of β-$Ni_2As_2O_7$, β-$Co_2As_2O_7$, and $Mn_2As_2O_7$ showing the hexagonal arrangement of MO_6 octahedra and AsO_4 tetrahedra (shaded).

z-direction. The As_2O_7 groups are in a staggered conformation (Figs. 7 and 8) so that the As ion from the opposite side of the As_2O_7 group shares two oxygens above and one below in the *z*-direction. Adjacent MO_6 octahedra along the *b*-axis share a pair of O2 atoms with distances of 2.050(1) Å (Ni–O2), 2.084(3) Å (Co–O2), and 2.16(2) Å (Mn–O2). The coordination octahedra are tetragonally elongated along the *a*-axis with (M–O3) bond lengths of 2.224(1) Å (Ni–O3), 2.260(1) Å (Co–O3), and 2.265(3) Å (Mn–O3). The remaining M–O bond lengths are 2.053(1) Å (Ni–O3), 2.074(2) Å (Co–O3), and 2.143(3) Å (Mn–O3).

The pyroarsenate anion consists of corner-shared tetrahedra with the bridging oxygen (O1) to arsenic distance, 1.647(1) Å (M = Ni), 1.656(2) Å (M = Co), and 1.687(3) Å (M = Mn). The As–O2 bond lies in the mirror plane and has a length of 1.697(1) Å (M = Ni), 1.676(2) Å (M = Co), and 1.67(3) Å (M = Mn). The remaining unique As–O bond length is 1.671(1) Å (M = Ni), 1.666(1) Å (M = Co), and 1.679(3) Å (M = Mn).

We note that β-$Ni_2As_2O_7$ is isomorphous with β-$Ni_2P_2O_7$ (*21*). It is interesting that three low temperature forms of $Ni_2P_2O_7$ are

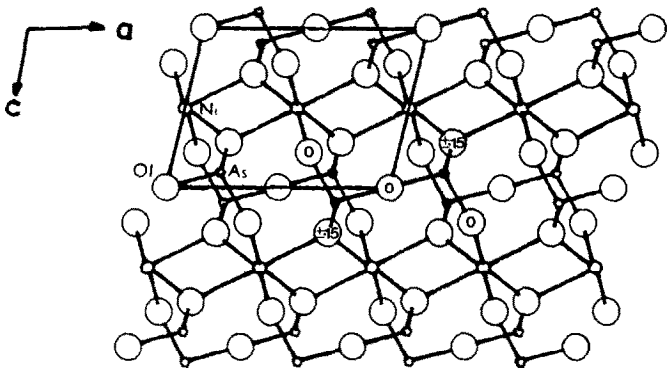

FIG. 8. Crystal structure of β-$Ni_2As_2O_7$, β-$Co_2As_2O_7$, and $Mn_2As_2O_7$. The atomic positions in one pyroarsenate group are marked.

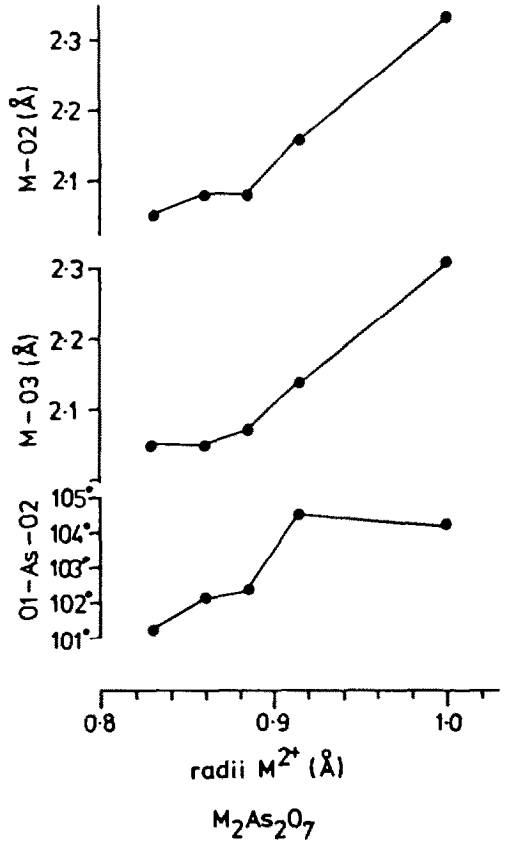

FIG. 9. Metal–oxygen bond lengths and O1–As–O angles for a series of transition metal pyroarsenates.

known; γ-$Ni_2P_2O_7$ (*22*), σ-$Ni_2P_2O_7$ (*23*), and α-$Ni_2P_2O_7$ (*22*). In the σ-form the O–P–O bond is linear.

4.2 High Temperature Structural Phase Transitions

Figure 9 shows metal–oxygen distances and O1–As–O angles for a series of transition metal pyroarsenates. In common with other structures of thortveitite analogs (e.g., *4, 16, 24*) the terminal O–As–O bond angles are larger than expected for a perfect tetrahedron, e.g., O2–As–O3 in β-$Co_2As_2O_7$ is 113.6°, and the O–As–O angles including the bridging oxygen atom are smaller, e.g., O1–As–O2 in β-$Co_2As_2O_7$ is 102.2°.

Two tetrahedral AsO_4 units may be connected by a linear As–O–As linkage. However, in this structure the geometry of the AsO_4 unit is governed by the bonding of the terminal oxygens to the metal ion. This means that to compensate for the linear As–O–As linkage, the AsO_4 groups must be compressed because the positions of the terminal oxygen atoms are primarily determined by the metal atoms and are therefore fixed. Furthermore, the shorter the *M*–O distance, the more distorted the AsO_4 tetrahedron and hence the greater the deviation of the terminal O–As–O1 bond angles from

109°. This is clearly in evidence in Fig. 9. The shortest M–O distances occur in those compounds with the smallest M^{2+} radius; for example, β-$Ni_2As_2O_7$ (Shannon and Prewitt (*25*), ionic radius Ni^{2+} = 0.83 Å) has M–O2 = 2.05 Å and the O1–As–O2 angle is 101.2°. For larger metal ions such as Mn^{2+} (ionic radius 0.97 Å (*25*)) the M–O bond lengths are greater (e.g., Mn–O2 = 2.16 Å in $Mn_2As_2O_7$ at 104.5°, and the O2–As–O1 bond angle is less distorted from 109°.

It seems likely that the distortion of AsO_4 in the β-phase compounds may play some part in the α–β-phase transition, thus the compounds with large metal ions (e.g., $Mn_2As_2O_7$ and $Ca_2As_2O_7$) have larger M–O distances and hence less distorted AsO_4 tetrahedra and do not exhibit the α–β-phase transition. It is those compounds with shorter M–O distances and more distorted AsO_4 tetrahedra that undergo the high temperature α–β-phase transition.

It is noteworthy that in all $M_2As_2O_7$ the anisotropic thermal factors of the bridging oxygen of the As_2O_7 group are large (Tables V and VII). Indeed, this behavior is observed for all β-phase pyroarsenates and pyrophosphates isomorphous with thortveitite. The origin of such large anisotropic temperature factors has been discussed in detail (e.g., *26*). It may be due to either a dynamic or static positional disorder. If the former, there would be enhanced thermal motion with its major component in the b-direction, perpendicular to the As–As bond direction. If the latter, the anion would be bent so that in half the unit cells O1 is displaced from the center of symmetry along the positive y direction and in the remainder, along the negative y direction. To refine the structure of the β-phase in terms of a disordered structure requires a knowledge of the crystal structure of the α-phase to generate the disordered structure.

It is apparent that the enhanced vibration of the bridging oxygen atom must play a key role in the α–β-phase transitions of metal pyroarsenates and pyrophosphates. In the low temperature (α) structures the X–O1–X (X = As or P) bond changes from a linear configuration in the β-phase to a bent one, e.g., 157° for α-$Cu_2P_2O_7$ (*26*) and 144° for α-$Mg_2P_2O_7$ (*27*). So, the α–β-phase transition may be envisaged as a "freezing out" of the thermal motion of the bridging oxygen atom in a potential well causing a bent X–O–X linkage. Coupled with this, one of the crystallographically equivalent

TABLE A

X-RAY POWDER DIFFRACTION PATTERN OF $Co_2As_2O_7$

I/I_{max} (× 10)	d_{obsd} (Å)	d_{calcd} (Å)	h	k	l
0.7	5.023	5.028	1	1	0
2.2	4.24	4.26	0	2	0
0.8	3.78	3.80	−1	1	1
9.5	3.15	3.17	1	−1	1
8.2	3.097	3.098	1	1	1
10.0	2.971	2.977	−2	0	1
1.1	2.616	2.619	1	−3	0
3.5	2.589	2.581	2	−2	0
0.7	2.569	2.566	1	3	0
2.7	2.53	2.51	2	2	0
0.1	2.448	2.444	0	−3	1
0.9	2.423	2.428	−2	−2	1
0.9	2.306	2.308	0	0	2
1.4	2.268	2.267	−1	1	2
0.3	2.204	2.205	1	−3	1
0.4	2.147	2.147	0	4	0
1.0	2.080	2.077	−1	−2	2
2.0	2.063	2.064	−2	1	2
0.6	1.919	1.919	−3	2	1
2.9	1.897	1.894	−3	−2	1
1.6	1.741	1.740	−2	4	1
0.8	1.721	1.722	3	1	1
0.9	1.695	1.691	−3	−3	1
2.2	1.669	1.668	1	−3	2
1.9	1.632	1.634	1	5	0
1.7	1.603	1.606	−4	1	1
1.6	1.538	1.539	0	0	3
1.2	1.518	1.519	2	−5	0
0.9	1.508	1.508	−2	−4	2
1.3	1.429	1.428	2	3	2
0.7	1.419	1.419	1	0	3
1.5	1.390	1.390	4	−1	1
0.9	1.375	1.375	−3	4	2

TABLE B

X-RAY POWDER DIFFRACTION PATTERN OF $Ni_2As_2O_7$

I/I_{max} (× 10)	d_{obsd} (Å)	d_{calcd} (Å)	h	k	l
0.6	4.94	5.04	1	1	0
1.9	4.16	4.23	−1	0	1
0.4	3.72	3.78	−1	1	1
10.0	3.12	3.15	1	−1	1
7.1	3.07	3.08	1	1	1
7.6	2.94	2.95	2	1	0
1.1	2.751	2.753	1	3	0
2.8	2.51	2.52	2	2	0
1.2	2.41	2.43	−2	−2	1
1.4	2.36	2.36	2	0	1
0.6	2.29	2.29	2	−1	1
1.3	2.255	2.253	2	1	1
0.4	2.194	2.195	0	1	2
0.6	2.131	2.131	−3	0	1
1.2	2.100	2.093	2	3	0
0.5	1.963	1.962	1	−1	2
0.7	1.948	1.953	0	−4	1
0.9	1.921	1.921	3	−2	0
0.6	1.898	1.898	−2	−2	0
1.2	1.877	1.879	3	2	0
0.4	1.759	1.762	0	3	2
0.8	1.736	1.742	3	−1	1
1.0	1.709	1.709	0	5	0
0.8	1.680	1.679	3	3	0
0.2	1.648	1.650	−3	2	2
1.6	1.620	1.616	1	3	2
1.0	1.582	1.579	0	−4	2
0.8	1.508	1.509	−3	−3	2
1.0	1.505	1.505	−2	−4	2
1.3	1.493	1.494	0	1	3
0.9	1.484	1.485	−4	0	2
0.7	1.386	1.386	−1	−3	3
1.1	1.379	1.375	4	1	1
0.6	1.364	1.365	−1	3	3
0.5	1.335	1.337	−3	2	3
0.6	1.321	1.322	−4	3	2
0.6	1.276	1.276	−1	−4	3

TABLE C

X-RAY POWDER DIFFRACTION PATTERN OF $Mn_2As_2O_7$

I/I_{max} (× 10)	d_{obsd} (Å)	d_{calcd} (Å)	h	k	l
1.2	5.13	5.26	1	1	0
0.2	4.32	4.38	0	2	0
0.2	3.28	3.29	2	0	0
0.8	3.21	3.23	1	1	1
1.1	3.19	3.20	0	2	1
0.2	3.02	3.02	2	0	−1
0.3	2.662	2.668	1	3	0
10.0	2.625	2.630	2	2	0
0.1	2.485	2.489	2	2	−1
0.2	2.448	2.449	2	0	1
0.05	2.230	2.234	1	3	1
0.1	2.124	2.127	3	1	0
0.2	1.803	1.822	2	4	0
0.1	1.797	1.797	3	1	1
0.1	1.773	1.773	2	4	−1
0.3	1.752	1.753	3	3	0
0.2	1.687	1.687	1	3	2
0.1	1.645	1.644	4	0	0
0.3	1.562	1.562	0	0	3
0.4	1.555	1.554	3	3	1
0.2	1.381	1.380	4	2	1
0.2	1.368	1.365	3	5	−1

M^{2+} ions may change from six- to fivefold coordination of oxygen ions. The phase transition involves a lowering of the crystal symmetry accompanied by enlargement of one or two of the unit cell axes. Thus for $M'_2X_2O_7$ (M' = Cu, X = P; M' = Mg, X = P; M' = Zn, X = As), the c-axis is doubled on going from the β-phase to the α-phase while the a-axis is unchanged, doubled and tripled, respectively (*26, 28, 29*). Since the structures of the α-forms of $Co_2As_2O_7$ and $Ni_2As_2O_7$ have not yet been determined fully, it is difficult to envisage possible mechanisms for the α–β-phase transition in these compounds. However, by analogy with other α-phase compounds, some multiplying of the unit cell axes must occur and the As–O–As linkage is likely to be bent.

Appendix

Tables of X-ray powder diffraction data for $M_2As_2O_7$; M = (a) Co, (b) Ni, and (c) Mn, at room temperature.

Acknowledgments

We thank N. Boseley of ICI Chemicals and Polymers Ltd., Runcorn for the DSC measurements, R. M.

Ibberson and W. I. F. David from the Rutherford Appleton Laboratory for assistance with the neutron diffraction experiments and data analysis, and M. J. Rosseinsky for interesting discussions. A.M.B. thanks ICI Chemicals and Polymers Ltd. and Balliol College, Oxford, for financial assistance. S.T.B. thanks Lincoln College Oxford for an E.P.A. Cephalosporin Junior Research Fellowship. We thank the S.E.R.C. for the provision of neutron scattering facilities at ISIS.

References

1. I. D. Brown and C. Calvo, *J. Solid State Chem.* **1,** 173–179 (1970).
2. R. W. G. Wyckoff, "Crystal Structures," Vol. 3, Wiley, New York (1960).
3. D. W. J. Cruickshank, H. Lynton, and G. A. Barclay, *Acta Crystallogr.* **15,** 491 (1962).
4. B. E. Robertson and C. Calvo, *Canad. J. Chem.* **46,** 605 (1968).
5. A. M. Buckley, D. Phil. Thesis, Oxford (1988).
6. J. B. Forsyth, C. Wilkinson, S. Paster, and B. M. Wanklyn, *J. Phys. Condens. Matter* **1,** 169–178 (1989).
7. M. F. Collins, G. S. Gill, and C. V. Stager, *Canad. J. Phys.* **49,** 979 (1971).
8. J. B. Taylor and R. B. Heyding, *Canad. J. Chem.* **36,** 597 (1958).
9. F. Fontan, M. Orliac, and F. Permingeat, *Bull. Soc. Fr. Mineral. Cristallogr.* **98,** 78–84 (1975).
10. J. S. Rollet, "Computing Methods in Crystallography," Pergamon, Elmsford, NY (1965).
11. M. W. Johnson and W. I. F. David, "Rutherford Appleton Laboratory Report," RAL-85-112 (1985).
12. H. M. Rietveld, *J. Appl. Crystallogr.* **2,** 65–71 (1969).
13. P. J. Brown and J. C. Matthewman, "Rutherford Appleton Laboratory Report," RAL-87-010 (1987).
14. J. Ozog, N. Krishnamachari, and C. Calvo, *Canad. J. Chem.* **48,** 388–399 (1970).
15. K. Tukaszewicz and R. Smajkioewicz, *Rocz. Chem.* **35,** 741 (1961).
16. C. Calvo and K. Neelakantan, *Canad. J. Chem.* **48,** 890–894 (1970).
17. P. J. Brown and J. C. Matthewman, "The Cambridge Crystallography Subroutine Library, Mark 3 User's Manual," RAL-87-010 (1987).
18. W. I. F. David, A. K. Akporiaye, R. M. Ibberson, and C. C. Wilson, "The HRPD at ISIS—An Introductory Users Guide," Version 1.0 (1989).
19. W. C. Hamilton, *Acta Crystallogr.* **18,** 502 (1965).
20. J. W. Visser, *J. Appl. Crystallogr.* **2,** 89 (1969).
21. A. Pietraszko and K. Lukaszewicz, *Bull. Acad. Pol. Sci. Chem.* **XVI,** 183–187 (1968).
22. K. Lukaszewicz, *Bull. Acad. Pol. Sci. Chem.* **XV,** 47–51 (1967).
23. R. Masse, J. C. Guitel, and A. Durif, *Mater. Res. Bull.* **14,** 337–341 (1979).
24. C. Calvo, *Canad. J. Chem.* **43,** 1139–1146 (1965).
25. R. D. Shannon and C. T. Prewitt, *Acta Crystallogr. B* **25,** 925 (1969); *Acta Crystallogr. B* **26,** 1046 (1970).
26. B. E. Robertson and C. Calvo, *Acta Crystallogr.* **22,** 665 (1967).
27. N. Krishnamachari and C. Calvo, *Acta Crystallogr. B* **28,** 2883 (1972).
28. C. Calvo, *Acta Crystallogr.* **23,** 289 (1967).
29. B. E. Robertson and C. Calvo, *J. Solid State Chem.* **1,** 120–133 (1970).